льних досліджень, апробація яких на ряді вугільних шахт Кузбасу підтверджує можливість їх практичного застосування.

Ключові слова: *антропогенні моделі, гірничопромислові системи, геоінформаційне моделювання*

Цель. Разработка методов геоинформационного моделирования антропогенных систем для повышения эффективности горного производства.

Методика. Построение антропогенных моделей горных предприятий и выбор эффективных вариантов решений с применением имитационного моделирования и ГИС-технологий.

Результаты. Установлено, что разработанные антропогенные модели позволяют наиболее полно описывать процессы горного производства.

Научная новизна. Заключается в использовании методов имитационного моделирования и ГИС-технологий при создании антропогенных моделей горнопромышленных систем, позволяющих обеспечить адекватное модельное представление основных объектов и процессов горного предприятия.

Практическая значимость. Разработаны основные типы антропогенных моделей и методика проведения модельных исследований, апробация которых на ряде угольных шахт Кузбасса подтверждает возможность их практического применения.

Ключевые слова: *антропогенные модели, горнопромышленные системы, геоинформационное моделирование*

Рекомендовано до публікації докт. техн. наук С.З. Шкундіним. Дата надходження рукопису 08.09.14.

Yinchuan Wu[1,2], Baolong Guo[1], Miaoyu Zhang[1]

1 –Xidian University, Xi'an, Shaanxi, China
2 – Xi'an Shiyou University, Xi'an, Shaanxi, China

INFLUENCE OF METAL CASING ON THE ELECTRIC FIELD IN A CASED HOLE

Іньчуань У[1,2], Баолун Го[1], Мяоюй Чжан[1]

1 – Університет Сідянь, м. Сіань, провінція Шеньсі, КНР
2 – Університет Сіань Шию, м. Сіань, провінція Шеньси, КНР

ВПЛИВ МЕТАЛЕВИХ ОБСАДНИХ ТРУБ НА ЕЛЕКТРИЧНЕ ПОЛЕ У СВЕРДЛОВИНІ

Purpose. To study the influence of metal casing parameters (casing conductivity and casing thickness) on the electrical field and the second derivative of potential in cased hole formation resistivity technology.

Methodology. The calculation formulas of the electrical field and the second derivative of potential were derived in multilayer media. Then the models of nondefective casing well and corrosion casing well were built in COMSOL soft. Moreover, both the electric field and the second derivative of potential were numerically calculated for nondefective casing well and corrosion casing well separately. Meanwhile, the influence of metal casing was analyzed.

Findings. The lower the conductivity of the metal casing is, the stronger the electric field and the second derivative of potential are; the electric field and the second derivative of potential are affected by metal casing parameters. These changes are always in close relation to corrosion defects in metal casing.

Originality. The models of cased hole were built in finite element analysis soft (COMSOL). The relation curve between the electrical field and casing parameters (conductivity and casing thickness) was obtained. The influence rule of metal casing was analyzed in detail.

Practical value. The results are applied to instrument design and logging interpretation.

Keywords: *electrical field, the second derivative of potential, corrosion metal casing, cased hole formation resistivity logging, cased hole model, COMSOL software*

Introduction. With Logging technology has been applied in the whole process of oil and gas exploration and development. The technology is an indispensable means of accurate oil and gas beds discovery and reservoir description, also provides important basis for reservoir determination, oil and gas reserves calculation, productivity evaluation and development planning, etc. Oil and gas reserves evaluation was based primarily on formation resistivity measurement, which has an irreplaceable engineering value for Hydrocarbons [1]. The traditional resistivity measurement was applied in open hole, and when the well was cased, compared with the formation resistivity, the metal casing resistivity was extremely small, therefore, the borehole resistivity logging instruments are not used in the casing well [2]. The cased hole logging is usually used in the old well, where the metal casing suffers from the high temperature, pressure and corrosion, defects such as holes, cracks, distortions, corrosions, fractures and collars will occur to the casing itself [3]. These defects influence the formation resistivity measurement, the logging response, when these defects are greatly serious, the logging data cannot be obtained, which makes the formation resistivity acquisition by logging interpretation impossible.

Previous research in this area includes as follows. In 1990, Kaufman [4] developed a theory to describe the elec-

tric field on the borehole axis in the presence of a conductive casing and investigate the behavior of the potential, the electric field, and the second derivative of the potential. In addition, the influence of the casing conductance and resistivity of the formation on the boundary of the intermediate zone is studied. In 2008, some experts illustrated the response of through-casing resistivity logging in heterogeneous-casing well [5–6]. The study found that the change of resistivity of the metal casing has an important effect on through-casing resistivity logging response, and the results show that the casing change whether thinner or thicker has an obvious effect on the logging responses, and the abnormality of logging response appears where the casing resistance suddenly decreases or increases. In 2013, Zhou [7] analyzed the effect of casing collar on formation resistivity logging through casing. The study found that the formation resistivity logging through is affected by thickness, length and electrical resistance per unit length of casing collar. In 2014, Liu [8] analyzed the effects of casing local variations on logging response. The numerical mode-matching method is first used to simulated through-casing resistivity logging response. The simulating results show that abnormal variations of logging response appear in and nearby inhomogeneous sections.

Different from the above research, based on the theoretical analysis of the electromagnetic field, this paper derives calculation formulas of the electric field and the second derivative of potential in multi-layer media. Moreover, the models of nondefective casing well and corrosion casing well are built in COMSOL, and the electric field and the second derivative of potential of cased hole are first studied by finite element analysis. The law of effect of casing conductance on the electrical field or the second derivative of potential is obtained. Meanwhile, the simulation results show that the changes of the electric field and the second derivative of potential are always in close relation to corrosion defects of the metal casing in cased hole. The results are applied to instrument design and logging interpretation.

Ectromagnetic field theory. ***The electric field distribution in the two-layer medium.*** Fig.1 is the two-layer medium model, assuming the borehole radius is a, the formation resistivity and the borehole resistivity are σ_f and σ_h respectively, point source A on the axis of the well and its current intensity I.

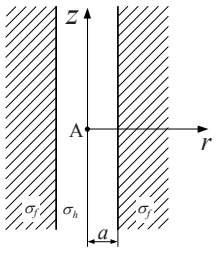

Fig. 1. Two-layer medium model

In the media, potential U and electric field E satisfy

$$E = -\text{grad}U. \tag{1}$$

According to (1), through resolving potential U, the electric field E is obtained. Under the two-layer medium condition, potential must satisfy the following:

(a) The potential U within the borehole and in the formation satisfies the Laplace equation

$$\nabla^2 U = 0; \tag{2}$$

(b) At the interface between the borehole and the formation, the potential U and the normal component of the current density are continuous functions; that is,

$$U_h\big|_{r=a^+} = U_f\big|_{r=a^-}; \tag{3}$$

$$-\sigma_h \cdot \frac{\partial U_h}{\partial r}\bigg|_{r=a^+} = -\sigma_f \cdot \frac{\partial U_f}{\partial r}\bigg|_{r=a^-}; \tag{4}$$

(c) Far from the point source, the potential tends to zero

$$U \to \frac{I}{4\pi\rho\sigma_h} \text{ as } \rho \to \infty; \tag{5}$$

(d) Near the point source A, the potential U tends to

$$U \to \frac{I}{4\pi\rho\sigma_h} \text{ as } \rho \to 0,$$

where ρ is the distance from measuring point to source A, then $\rho = \sqrt{r^2 + z^2}$.

The two-layer medium chooses cylindrical coordinates, its origin is at point A, axis z coincides with well axis. Because the medium is of axial symmetry, the potential is irrelevant to the angle φ, (2) changes to

$$\frac{\partial^2 U}{\partial r^2} + \frac{1}{r} \cdot \frac{\partial U}{\partial r} + \frac{\partial^2 U}{\partial z^2} = 0. \tag{6}$$

Applying the method of separation of variables, (6) can be resolved as

$$U(r,z) = \int_0^\infty [A_1(\lambda) I_0(\lambda r) + A_2(\lambda) K_0(\lambda r)] \cos \lambda z d\lambda, \tag{7}$$

where $I_0(\lambda r)$ is the first modification of zero order Bessel function, $K_0(\lambda r)$ the second modification of zero order Bessel function, $A_1(\lambda)$ and $A_2(\lambda)$ are unknown coefficients, and in different media, the coefficients value is different. When $r \to 0$, the second modification of zero order Bessel function $K_0(\lambda r) \to \infty$. To meet continuous potential conditions within the borehole, only when $A_2(\lambda) = 0$, potential U_h in the well is

$$U_h(r,z) = \frac{I}{4\pi\sigma_h} \cdot \frac{1}{\rho} + \int_0^\infty A_1(\lambda) I_0(\lambda r) \cos \lambda z d\lambda. \tag{8}$$

According to the integral formula, here is identical equation

$$\frac{1}{\rho}=\frac{2}{\pi}\int_0^\infty K_0(\lambda r)\cos\lambda z d\lambda. \tag{9}$$

Substituting (9) into (8), there is

$$U_h(r,z)=\frac{I}{2\pi^2\sigma_h}\int_0^\infty K_0(\lambda r)\cos\lambda z d\lambda + \\ +\int_0^\infty A_1(\lambda)I_0(\lambda r)\cos\lambda z d\lambda.$$

When $r\to\infty$, $I_0(\lambda r)\to\infty$, to meet potential conditions of (5) in (7), $A_1(\lambda)=0$. Therefore, the potential U_f within formation is

$$U_f(r,z)=\int_0^\infty A_2(\lambda)K_0(\lambda r)\cos\lambda z d\lambda.$$

To determine the coefficients $A_1(\lambda)$ and $A_2(\lambda)$ in U_h and U_f, in accord with (3) and (4), there is

$$\frac{I}{2\pi^2\sigma_h}\int_0^\infty K_0(\lambda a)\cos\lambda z d\lambda+\int_0^\infty A_1(\lambda)I_0(\lambda a)\cos\lambda z d\lambda= \\ =\int_0^\infty A_2(\lambda)K_0(\lambda a)\cos\lambda z d\lambda; \tag{10}$$

$$\sigma_h\left[-\frac{I}{2\pi^2\sigma_h}\int_0^\infty K_1(\lambda a)\lambda\cos\lambda z d\lambda+\int_0^\infty A_1(\lambda)I_1(\lambda a)\lambda\cos\lambda z d\lambda\right]= \\ =-\sigma_f\int_0^\infty A_2(\lambda)K_1(\lambda a)\lambda\cos\lambda z d\lambda, \tag{11}$$

where $I_1(x)$ is the first modification of first order Bessel function, $K_1(x)$ the second modification of first order Bessel function. And there is

$$\begin{cases} I_1(x)=I_0'(x) \\ K_1(x)=-K_0'(x) \end{cases},$$

(10) and (11) meet all *z* axes, so there is

$$\begin{cases} \frac{I}{2\pi^2\sigma_h}K_0(\lambda a)+A_1(\lambda)I_0(\lambda a)=A_2(\lambda)K_0(\lambda a) \\ -\frac{I}{2\pi^2}K_1(\lambda a)+\sigma_h A_1(\lambda)I_1(\lambda a)=-\sigma_f A_2(\lambda)K_1(\lambda a) \end{cases}.$$

The coefficient $A_1(\lambda)$ to be

$$A_1(\lambda)=\frac{I}{4\pi\sigma_h}\cdot\frac{2}{\pi}\cdot\frac{\lambda a P_h K_0(\lambda a)K_1(\lambda a)}{1+\lambda a P_h K_0(\lambda a)K_1(\lambda a)}, \tag{12}$$

where $P_h=\frac{\sigma_h-\sigma_f}{\sigma_f}$. Putting (12) into (8), here is

$$U_h(r,z)=\frac{I}{4\pi\sigma_h}\cdot\frac{1}{\rho}+ \\ +\frac{I}{4\pi\sigma_h}\cdot\frac{2}{\pi}\int_0^\infty\frac{\lambda a P_h K_0(\lambda a)K_1(\lambda a)}{1+\lambda a P_h K_0(\lambda a)K_1(\lambda a)}I_0(\lambda r)\cos\lambda z d\lambda.$$

When $r=0$, the potential at the well axis is

$$U_h(0,z)=\frac{I}{4\pi\sigma_h}\cdot\frac{1}{z}+ \\ +\frac{I}{4\pi\sigma_h}\cdot\frac{2}{\pi}\int_0^\infty\frac{\lambda a P_h K_0(\lambda a)K_1(\lambda a)}{1+\lambda a P_h K_0(\lambda a)I_1(\lambda a)}\cos\lambda z d\lambda.$$

Combined with (1), when $r=0$, the electric field at the well axis is

$$E_{hz}(0,z)=-\frac{\partial U_m}{\partial z}=\frac{I}{4\pi\sigma_h}\cdot\frac{1}{z^2}+ \\ +\frac{I}{4\pi\sigma_h}\cdot\frac{2}{\pi}\int_0^\infty\frac{\lambda^2 a P_h K_0(\lambda a)K_1(\lambda a)}{1+\lambda a P_h K_0(\lambda a)K_1(\lambda a)}\sin\lambda z d\lambda.$$

The second derivative of potential is

$$\frac{\partial^2 U_h}{\partial z^2}=\frac{I}{4\pi\sigma_h}\cdot\frac{2}{z^3}- \\ -\frac{I}{4\pi\sigma_h}\cdot\frac{2}{\pi}\int_0^\infty\frac{\lambda^3 a P_h K_0(\lambda a)K_1(\lambda a)}{1+\lambda a P_h K_0(\lambda a)K_1(\lambda a)}\cos\lambda z d\lambda.$$

The electric field distribution in the two-layer medium. Fig. 2 is the three-layer medium model, assuming the borehole radius is a, the casing thickness Δa, the resistivity of the borehole, the casing and formation are σ_h, σ_c and σ_f respectively, putting point source *A* on the axis of well and its current intensity being I.

Making use of the above method and cylindrical coordinates, the potential at the well axis is

$$U_h(0,z)=\frac{I}{4\pi\sigma_h}\cdot\frac{1}{z}+\frac{I}{4\pi\sigma_h}\cdot\frac{2}{\pi}\int_0^\infty A(\lambda)\cos\lambda z d\lambda.$$

The electrical field at the axis is

$$E_{hz}(0,z)=-\frac{\partial U_m}{\partial z}=\frac{I}{4\pi\sigma_h}\cdot\frac{1}{z^2}+ \\ +\frac{I}{4\pi\sigma_h}\cdot\frac{2}{\pi}\int_0^\infty\lambda A(\lambda)\sin\lambda z d\lambda. \tag{13}$$

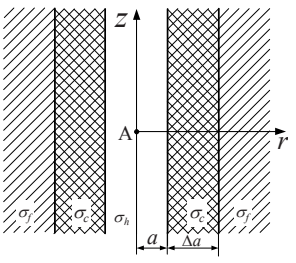

Fig. 2. Three-layer medium model

The second derivative of potential difference is

$$\frac{\partial^2 U_h}{\partial z^2} = \frac{I}{4\pi\sigma_h}\cdot\frac{2}{z^3} - \\ -\frac{I}{4\pi\sigma_h}\cdot\frac{2}{\pi}\int_0^\infty \lambda^2 A(\lambda)\cos\lambda z d\lambda. \quad (14)$$

Where

$$A(\lambda) = \frac{C(\lambda) + xPK_1(x)[K_0(x) + C(\lambda)I_0(x)]}{1 + xPI_1(x)[K_0(x) + C(\lambda)I_0(x)]};$$

$$C(\lambda) = \frac{x_c P_c K_0(x_c) K_1(x_c)}{1 + x_c P_c K_0(x_c) I_1(x_c)};$$

$$x = \lambda \cdot a;$$

$$x_c = \lambda \cdot a';$$

$$P = \frac{\sigma_m - \sigma_c}{\sigma_c};$$

$$P_c = \frac{\sigma_c - \sigma_f}{\sigma_f}.$$

In the casing well, according the distance from the measuring point to source point *A*, the electrical field can be divided into: the near zone, intermediate zone and far zone. The logging is conducted in the intermediate zone ($10 < z/a < 10^3$), at this moment (13) and (14) can be written as [9]

$$E_{hz}(0,z) \approx \frac{I}{2S_c} e^{-z/\sqrt{S_c/\sigma_f}}; \quad (15)$$

$$\frac{\partial^2 U_h}{\partial z^2} \approx \frac{I}{2S_c^{3/2}}\sqrt{\sigma_f}\cdot e^{-z/\sqrt{S_c/\sigma_f}}. \quad (16)$$

Where S_c, the casing conductance can be written as

$$S_c = 2\pi \cdot a \cdot \Delta a \cdot \sigma_c.$$

From (15) and (16), it can be seen that: at the well axis, the electrical field and the second derivative of potential in the intermediate zone are mainly determined by exciting currents, the formation conductance, and the casing conductance. Therefore, the formation resistivity can be obtained by measuring the second derivative of potential. When there is a defect in the casing, combining and solving above functions is very difficult, we have only to consider numerical computation method.

The casing well model. Different from open hole model, the computational domain of cased hole model was large (thousands of meters), which caused great difficulties to the large-scale calculation; besides, the ratio between the casing conductivity and the formation conductivity was between 10^6–10^{10}, which made the numerical calculation convergence more difficult [10].

The model of nondefective casing well. We apply the cylindrical coordinates to the casing well modeling, which satisfies the axis-symmetrical conditions. Therefore, the three-dimensional model can be simplified into the two-dimensional one. Fig. 3 is the nondefective casing well model. The casing well consists of three medium: borehole (its electrical conductivity, σ_h), casing (its electrical conductivity, σ_c) and formation (its electrical conductivity, σ_f). In this model, the borehole radius (the inside casing radius) is a, casing thickness Δa, the radius of model L, the height of model H.

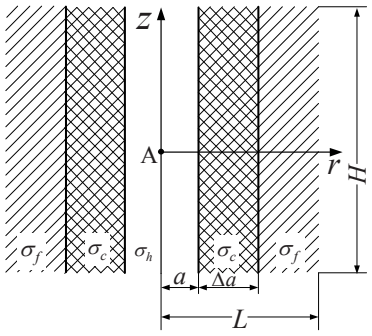

Fig. 3. Model of the cased hole with the nondefective casing

The model of defective casing well. Fig. 4 is the model of internal uniform corrosion casing well, the thickness of corrosion section reduces from Δa to Δa_1, and the corrosion height is h_1. Fig. 5 is the model of external uniform corrosion casing well, the thickness of corrosion section reduces from Δa to Δa_2, and the corrosion height is h_2.

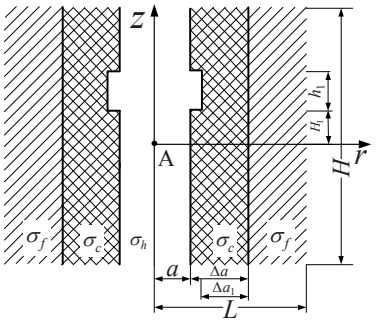

Fig. 4. Model of the cased hole with the internal uniform corrosion casing

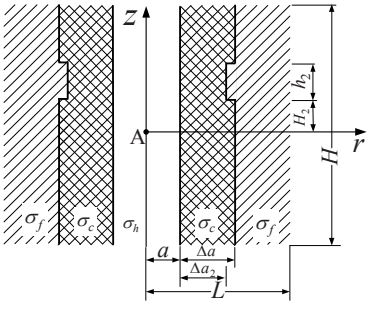

Fig. 5. Model of the cased hole with the external uniform corrosion casing

The numerical calculation results analysis. In the numerical calculation model, the borehole radius $a = 0.1$ m, the casing thickness $\Delta a = 0.01$ m, the formation radius $L = 2000$ m, the formation thickness $H = 4000$ m, the borehole electrical conductivity $\sigma_h = 0.1$ S/m, the formation elec-

trical $\sigma_f = 0.1$ S/m. The exciting current source is the ring current source ($r = 0.1$ m, $z = 0$ m), which closely clings to the internal casing wall, is 10A/m, and the outermost part of model is chosen as the return ground terminal. Making use of the multi-physical field analysis software (COMSOL) to set up the systemic model, subdivide the grid finely and reasonably, and analyze influences of changes in casing parameters on electrical field distribution characteristics through numerical calculation results analysis.

The electrical field distribution of nondefective casing well. It is shown as fig. 3, the casing conductivity σ_c is 1×10^4 S/m, 2×10^4 S/m, 1×10^5 S/m, 2×10^5 S/mand 1×10^6 S/m respectively. And under different conditions, we study distribution characteristics of the potential, the electrical field and the second derivative of potential of the model.

The potential distribution of nondefective casing well. The potential distribution of nondefective casing well is obtained as is shown in fig. 6–8.

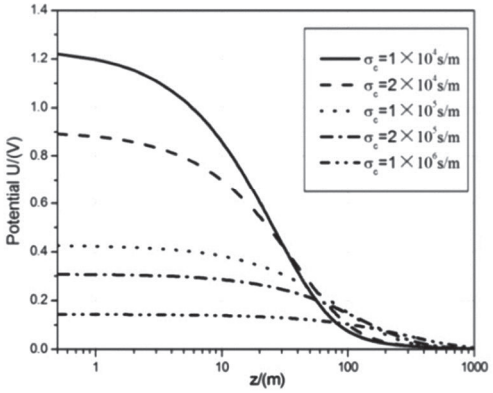

Fig. 6. Potential distribution along axis z ($r = 0$ m) in the cased hole with the nondefective casing

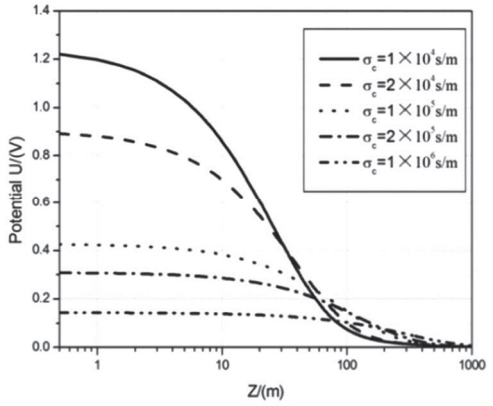

Fig. 7. Potential distribution along axis z ($r = 0.1$ m) in the cased hole with the nondefective casing

On the well axis ($r = 0$ m), with different casing conductivities, the potential distributes along axis z, ($z = 0.5 - 1000$ m), which is shown as fig. 6. On the internal casing wall ($r = 0.1$ m), with different casing conductivities, the potential distributes along axis z ($z = 0.5 - 1000$ m) as is shown in fig. 7.When $z = 1$ m, with different casing conductivities, the potential distributes along axis r ($r = 0.01 - 100$ m) as is shown in fig. 8. From fig. 6–8, one can see that: when the casing electrical conductivity is different, the potential is different, the potential will reduce as distance r increases; when r remains unchanged (shown as fig. 6 or 7), within the range ($z < 30$ m), the larger the casing conductivity is, the smaller the potential is; when z is determined (fig. 8), within the range ($r < 0.11$ m), when the casing conductivity is the same, the potential basically remains unchanged, i.e. between the well axis and outer wall of casing ($0 < r < 0.11$ m), when z is the same, the potential remains the same, so there are the same potential distribution characteristics in fig. 6, 7.

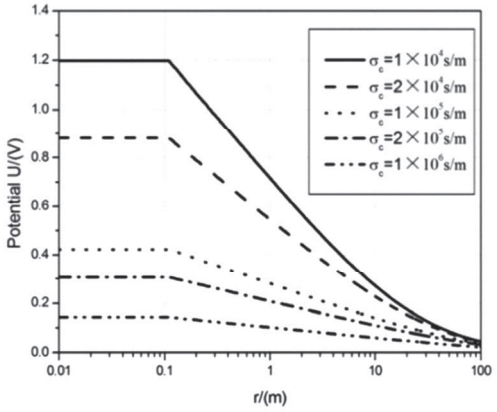

Fig. 8. Potential distribution along axis r ($z = 1$ m) in the cased hole with the nondefective casing

The electrical field distribution of nondefective casing well. The electrical field distribution of nondefetive casing well is shown as fig. 9–12. Fig. 9 shows on the casing internal wall ($r = 0.1$ m), the distribution of E_z along axis z ($z = 0.5 - 1000$ m), as z becomes larger, the electrical field E_z turns smaller; within the range ($z < 50$ m), the bigger the casing electrical conductivity, the smaller the field is. Fig. 12 shows: when $z = 1$ m, within the range ($r = 0.01 - 0.11$ m), electrical field E_z of the same conductivity remains the same; through casing, after getting into the formation ($r > 0.11$ m), as the radial distances (r) increases, electrical field E_z decreases; within the range ($r < 20$ m), the bigger the conductivity is, the smaller the electrical field is.

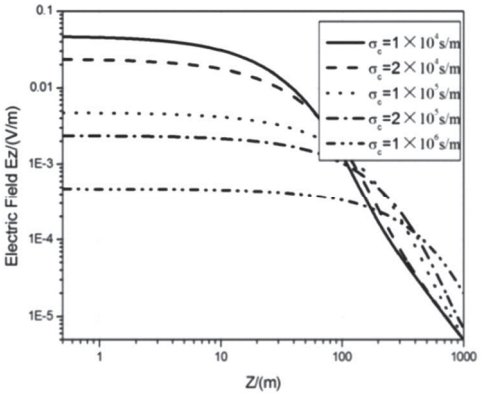

Fig. 9. Electric fiel E_z distribution along axis z ($r = 0.1$ m) in the cased hole with the nondefective casing

Fig. 13 shows: within the borehole, the order of the electrical field E_r is very small, for instance, when $z = 1$ m, $\sigma_c = 1 \times 10^6$ s/m, the order of the electrical field E_r is among 10^{-12}–10^{-11},while that of E_z is among 10^{-4}–10^{-3}, so E_r is negligible within the borehole; within the range ($z < 70$ m), the bigger the casing conductivity is, the smaller E_r is.

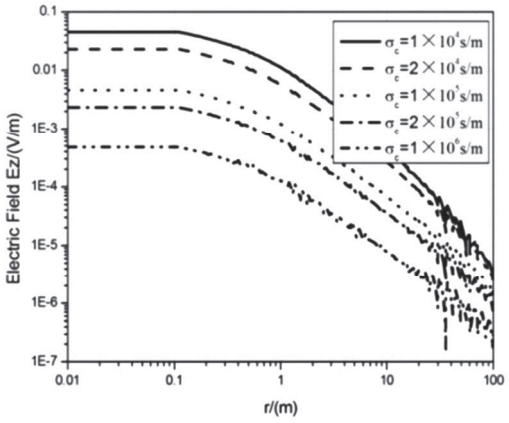

Fig. 10. Electrical field E_z distribution along axis r ($z = 1$ m) in the cased hole with the nondefective casing

Fig. 12 shows: when $z = 1$ m, within the borehole ($r = 0.01 - 0.1$ m), as r becomes larger, E_r gradually increases, when at the same r, the bigger the conductivity is, the larger the E_r becomes; after getting into the metal casing ($r = 0.1 - 0.11$ m), sharp jumping changes occur to E_r; after leaving from the casing and entering into the formation ($r > 0.11$ m), as r increases, E_r becomes smaller.

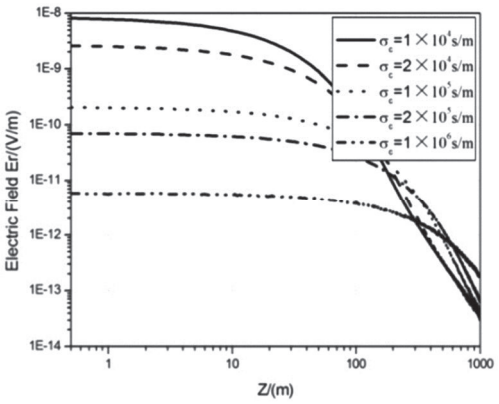

Fig. 11. Electrical field E_r distribution along axis z ($r = 0.1$ m) in the cased hole with the nondefective casing

The second derivative of potential distribution of non-defective casing well. According to theoretical analysis, in the actual logging, by measuring the second derivative of potential, we make use of the formula to work out the formation electrical conductivity. Fig. 13 shows on the internal casing wall ($r = 0.1$ m), the second derivative of potential distribution along axis z ($z = 0.5 - 1000$ m): when $z < 80$ m, the bigger the conductivity is, the smaller the second derivative of potential is; for instance, when $z = 1$ m, $\sigma_c = 1 \times 10^6$ s/m, the second order potential is about 10^{-6}; as z increases, the second derivative of potential gradually decreases, the bigger the conductivity is, the smaller the second derivative of potential is. In the actual logging instrument design, the size of the second derivative of potential directly influences the resolution of acquisition system; the smaller the second derivative of potential is, the higher the resolution of the acquisition system, the more difficult the instrument design is.

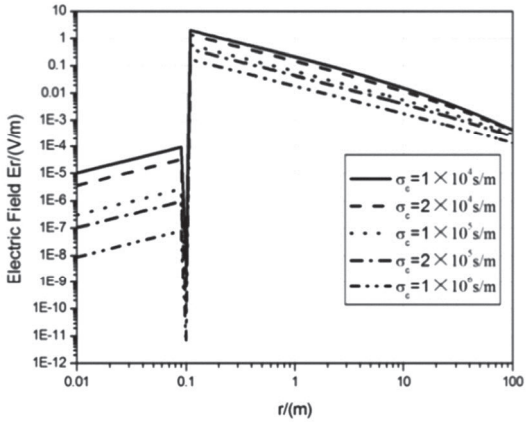

Fig. 12. Electrical field E_r distribution along axis r ($z = 1$ m) in the cased hole with the nondefective casing

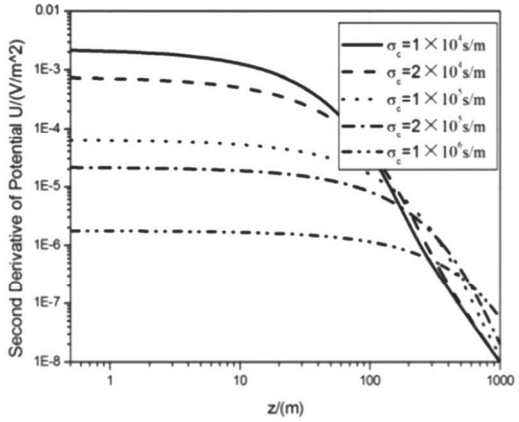

Fig. 13. Second derivative of potential distribution along axis z ($r = 0.1$ m) in the cased hole with the nondefective casing

Synthesizing the above analysis, the following can be obtained: inside the casing well ($r = 0 - 0.11$ m), when z point is the same, the potential U, the electrical field E_z, and the second derivative of potential at the radial r direction are the same; inside the casing well ($r = 0 - 0.1$ m), the electrical field E mainly distributes along axis z, at the r direction, E_r is negligible; inside the formation, ($r > 0.11$ m), the electrical field E mainly distributes along axis r towards direction of E_r; inside the metal casing ($r = 0.1 - 0.11$ m) sudden changes occur to E_r along the radial direction r, then make the electrical field E_r inside the formation much bigger than that of E_r inside the well. Therefore, inside the casing well, only distributions characteristics of potential, the electrical field and the second derivative of potential along the vertical direction z are studied, the measuring point can be

any one from the well axis to the internal wall of casing, in all the following cased holes with the defective casing, the well axis is chosen as the measuring point.

The electrical field analysis of cased well with the uniform corrosion casing. The uniform corrosion of casing includes internal and external wall corrosions, and the model is shown as fig. 4–5. In fig. 4, $H_1 = 3.0$ m, $h_1 = 0.5$ m, $\Delta a_1 = 0.05$ m. In fig. 5, $H_2 = 3.0$ m, $h_2 = 0.5$ m, $\Delta a_2 = 0.05$ m. In the models, when the casing conductivity σ_c (2×10^4 S/m, 2×10^5 S/m, 2×10^6 S/m) is different, we study distribution characteristics of the electrical field and the second derivative of potential difference along the axis z, which are shown as fig. 14–17. Through the contrastive observation, under the two kinds of corrosion conditions, distributions of electrical field and the second derivative of potential difference are almost correspondingly the same, and directly from the curves, it cannot be identified whether the casing is of internal or external corrosion. Through distribution of electrical field and the second derivative of potential difference, the corrosion position can be located. From fig. 15, it can be seen that the range where sudden changes of the second derivative of potential corresponds to the located corrosion sections; the smaller the casing conductivity is, the greater the variation extent of electrical field and the second derivative of potential of the corrosion section is; the electrical field curve of defective section approximately distributes symmetrically on the left and right sides at z=3.25m, which presents in parabolic shape, and at the defective part, the electrical field becomes greater, the maximum being at z=3.25m. From fig. 15, 17, we can see that the second derivative of potential curve of defective section approximately distributes symmetrically about the center of z (z=3.25m), which presents in sine shape, and at the boundaries of defective parts (z=3m, z=3.5m), the variation of the second derivative of potential is the greatest; Except for the distribution curves of the electrical field and the second derivative of potential of the defective sections, the curves of other sections are the same as those of other sections of the nondefective casing.

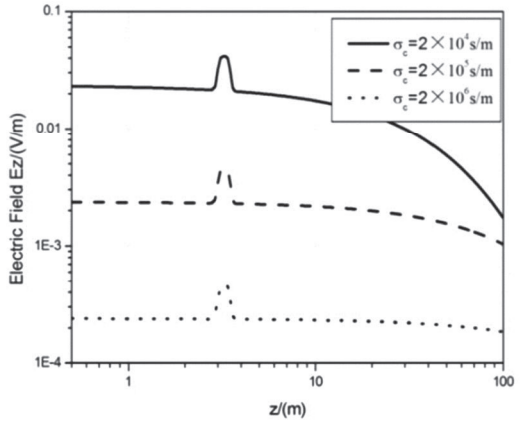

Fig. 14. Electrical field distribution along axis z ($r = 0$ m) in the cased hole with the internal uniform corrosion casing

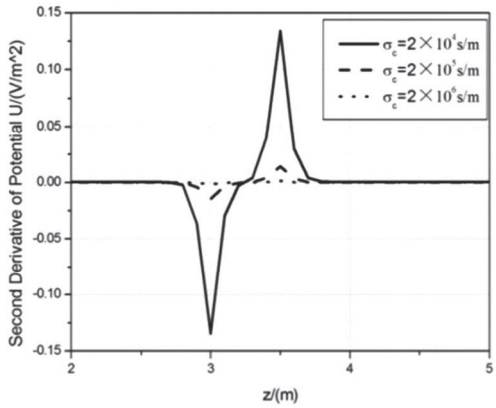

Fig. 15. Second order potential distribution along axis z ($r = 0$ m) in the cased hole with the internal uniform corrosion

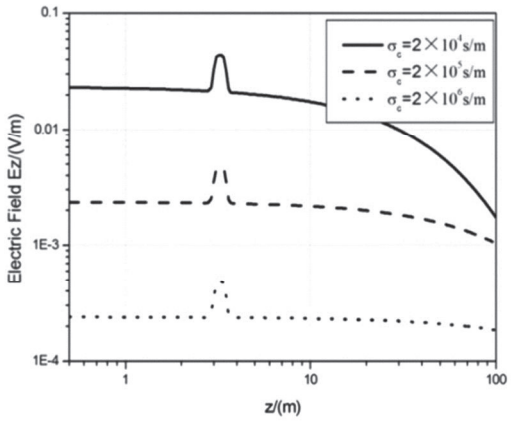

Fig. 16. Electrical field distribution along axis z ($r = 0$ m) in the cased hole with the external uniform corrosion

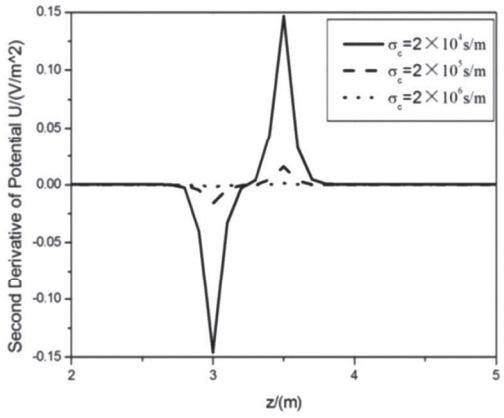

Fig. 17. Second order potential along axis z ($r = 0$ m) in the cased hole with the internal uniform corrosion

Conclusion. The measurement result of the second derivative of potential directly affects the calculation of formation resistivity in field logging. The lower the conductivity of the metal casing is, the stronger the electric field and the second derivative of potential are; the electric field and the second derivative of potential are affected by metal casing corrosion; these changes are always in close relation to corrosion defects in metal casing; the distribution of the

electric field is similar whenever the corrosion is located in internal or external wall of the metal casing. The results are applied to instrument design and logging interpretation.

Acknowledgements. This work was supported by Nation Science and Technology Major Project of the Ministry of Science and Technology of China (No. 2011ZX05020-004).

References / Список літератури

1. Wu, Y.C., Zhang, J.T. and Yan, Z.G. (2006), "An overview of the logging technology of formation resistivity through casing", *China Petroleum Instruments*, vol. 20, no.5, pp. 1−5.

2. B. Wenzhuo C. Mingyu Z.Wei. (2012), "A Verification and Validation Method for Calculation Model of Space", *Acta optica sinica*, vol.30, no.11, pp. 2249−2255.

3. Yang, Y., Liu, S.H., Li, F. (2013), "Research progress in casing detection technology", *China Petroleum Machinery*, vol. 41, no.8, pp. 17−22.

4. Wang, C.R., Li, Z.H., Wang, C.J. (2012), "Study and application of the new casing inspection combination well logging technology in Tuha oilfield", *China Petroleum Instruments*, vol.26, no.1, pp. 45−47.

5. Kaufman, A.A. (1990), "The Electrical Field in a Borehole with a Casing", *Geophysics*, vol. 55, no.1, pp. 29−38.

6. Gao, J., Liu, F.P., Bao, D.Z. (2008), "Responses simulation of through-casing resistivity logging in heterogeneous-casing wells", *Chinese Journal of Geophysics*, vol. 51, no.4, pp. 1255−1261.

7. Zhou, J.H., Wang, L., Yuan, R. (2013), "Analysis on Effect of Casing Collar on Formation Resistivity Logging Through Casing", *Progress in Geophysis* (in Chinese), vol. 28, no.1, pp. 421−426.

8. Liu, Y., Liu, G.Q. (2014), "Numerical simulation and analysis on the influence of casing inhomogeneity on through-casing resistivity logging response", *Chinese Journal of Geophysics*, vol. 57, no.4, pp. 1345−1355.

9. Gao, J., Ke, S.Z., Wen, B.J. (2010), "Introduction to numerical simulation of electrical logging and its development trend", Well Logging Technology (in Chinese), vol. 34, no.1, pp. 1−5.

10. Wu, Y.C., Guo, B.L., Zhang, J.T. (2014), "Response characteristics of cased hole formation resistivity logging", *International Journal of Earth Science and Engineering*, vol. 7, no.5, pp. 2075−2081.

Мета. Для досліджування впливу параметрів металевої обсадки (провідності обсадки та її товщини) на електричне поле та другу похідну потенціалу за технології формування опору у свердловині з обсадкою.

Методика. Розрахункові формули електричного поля та другої похідної потенціалу отримані в багатошаровому середовищі. Потім моделі недеформованих свердловин з обсадкою та свердловин з обсадкою при корозії побудовані у програмі COMSOL. Крім того, і електричне поле, і друга похідна потенціалу розраховані для недеформованої свердловини з обсадкою та свердловини з обсадкою при корозії окремо. При цьому аналізується вплив металевої обсадки.

Результати. Чим нижче провідність металевої обсадки, тим сильніше електричне поле та друга похідна потенціалу; металева обсадка впливає на параметри електричного поля та другу похідну потенціалу; ці зміни завжди у тісному зв'язку з дефектами корозії в металевій обсадці.

Наукова новизна. Моделі свердловин з обсадкою побудовані у програмі кінцево-елементного аналізу (COMSOL). Застосовується співвідношення між кривою електричного поля та параметрами обсадки (провідність і товщина). У деталях аналізується правило впливу металевої обсадки.

Практична значимість. Отримані результати застосовуються для проектування інструмента, а також каротажної інтерпретації.

Ключові слова: *електричне поле, друга похідна потенціалу, корозія металевої обсадки, каротаж за методом питомого опору пласта у свердловині з обсадкою, модель свердловини з обсадкою, програмне забезпечення COMSOL*

Цель. Для изучения влияния параметров металлической обсадки (проводимости обсадки и ее толщины) на электрическое поле и вторую производную потенциала при технологии формирования сопротивления в скважине с обсадкой.

Методология. Расчетные формулы электрического поля и второй производной потенциала получены в многослойной среде. Затем модели недеформированных скважин с обсадкой и скважин с обсадкой при коррозии построены в программе COMSOL. Кроме того, и электрическое поле, и вторая производная потенциала рассчитаны для недеформированной скважины с обсадкой и скважины с обсадкой при коррозии отдельно. При этом анализируется влияние металлической обсадки.

Выводы. Чем ниже проводимость металлической обсадки, тем сильнее электрическое поле и вторая производная потенциала; металлическая обсадка влияет на параметры электрического поля и вторую производную потенциала; эти изменения всегда в тесной связи с дефектами коррозии в металлической обсадке.

Научная новизна. Модели скважин с обсадкой построены в программе конечно-элементного анализа (COMSOL). Применяется соотношение между кривой электрического поля и параметрами обсадки (проводимость и толщина). В деталях анализируется правило влияния металлической обсадки.

Практическая значимость. Полученные результаты применяются для проектирования инструмента, а также каротажной интерпретации.

Ключевые слова: *электрическое поле, вторая производная потенциала, коррозия металлической обсадки, каротаж методом удельного сопротивления пласта в скважине с обсадкой, модель скважины с обсадкой, программное обеспечение COMSOL*

Рекомендовано до публікації докт. геол. наук М.М. Довбнічем. Дата надходження рукопису 15.09.14.